

Steering Organizational and Conformational Surface Chirality by Controlling Molecular Chemical Functionality

Christian Bombis,[†] Sigrid Weigelt,[†] Martin M. Knudsen,[‡] Martin Nørgaard,[†] Carsten Busse,[†] Erik Lægsgaard,[†] Flemming Besenbacher,[†] Kurt V. Gothelf,[‡] and Trolle R. Linderoth^{†,*}

[†]Interdisciplinary Nanoscience Center (iNANO) and Department of Physics and Astronomy, Aarhus University, 8000 Aarhus C, Denmark, and [‡]Interdisciplinary Nanoscience Center (iNANO), Danish National Research Foundation: Centre for DNA Nanotechnology (CDNA) and Department of Chemistry, Aarhus University, 8000 Aarhus C, Denmark

The self-assembly of supramolecular structures on metallic surfaces has been studied intensively during the past decade.¹ Particular interest has been devoted to chiral surface assemblies^{2,3} which is motivated both by fundamental interest in surface chirality and by the many potential applications within areas such as chiral specific sensors, enantiomeric separation, and asymmetric heterogeneous catalysis.

To control molecular self-assembly on 2D surfaces it is of utmost importance to have a detailed fundamental understanding of the delicate interplay between molecule–molecule and molecule–substrate interactions as well as to develop the ability to design and synthesize molecular building blocks with specific functional groups that can direct the formation of desired molecular nanoarchitectures.^{4,5} A strategy that has often been applied is to utilize planar aromatic molecules that adsorb parallel to the surface and implement functional groups designed to interact through specific and directional intermolecular hydrogen bonds^{5–12} or dipole–dipole forces.⁴ Molecules interacting primarily *via* less directional van der Waals forces are often found to form close-packed structures and competing, metastable, molecular phases,^{13–15} where the adsorption patterns depend primarily on the molecular geometry¹⁶ or stoichiometry.¹⁷

Chirality is often manifested in supramolecular surface structures. Most obviously, this occurs for intrinsically chiral compounds that transfer their chirality to the

ABSTRACT Molecular chirality on surfaces has been widely explored, both for intrinsically chiral molecules and for prochiral molecules that become chiral upon adsorption due to the reduced symmetry which follows from surface confinement. However, little attention has been devoted to chiral effects that originate from conformational degrees of freedom for adsorbed molecules. Here we have used scanning tunneling microscopy to investigate the self-assembled structures formed when a class of six linear, organic molecules (oligo-phenylene-ethynylenes) are adsorbed on a Au(111) surface under ultrahigh vacuum conditions. All of the investigated compounds are intrinsically achiral, but most display conformational chirality in the sense that the molecules can adsorb on the surface in different conformations giving rise to either one of two chiral surface enantiomers or a mirror-symmetric achiral meso form. A total of eleven observed adsorption structures are systematically investigated with respect to *conformational chirality* as well as *point chirality* (arising where molecular adsorption locally breaks the substrate symmetry) and *organizational chirality* (arising from the tiling pattern of the molecular backbones). A number of interesting correlations are identified between these different levels of chirality. Most importantly, we demonstrate that it is possible through control of the terminal group functionalization to steer the oligo(phenylene-ethynylene) molecular backbones into surface assemblies that either display pronounced organizational chirality or have mirror symmetric tiling patterns, and that it is furthermore possible to control the conformational surface chirality so the compounds preferentially assume either chiral or achiral surface conformers.

KEYWORDS: STM · self-assembly · chirality · molecular conformation · oligo(phenylene-ethynylene)s · organic synthesis

substrate upon adsorption.^{18–20} However, surface chirality can also emerge for adsorbates that are intrinsically achiral, and in Figure 1 is depicted a number of important ways in which this can occur.^{2,3} Even highly symmetric adsorbates can induce point chirality, provided they adsorb in such a way that the molecule–surface system in combination does not have any mirror symmetry elements²¹ (Figure 1a). Organizational chirality arises on the surface if the molecular arrangement in itself results in tiling patterns that are chiral, that is, are non-superimposable on their mirror-image forms by rotations and translations in the

See the accompanying Perspective by Gellman on p 5.

*Address correspondence to trolle@inano.au.dk.

Received for review September 23, 2009 and accepted December 04, 2009.

Published online December 15, 2009. 10.1021/nn9012803

© 2010 American Chemical Society

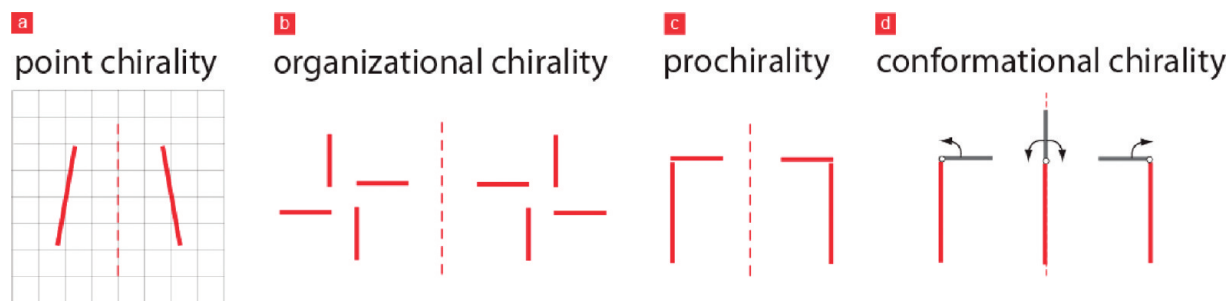


Figure 1. Different levels of molecular surface chirality arising for intrinsically achiral adsorbates. (a) Point chirality arises if the molecule–surface system in combination possesses chirality, as illustrated schematically for a rod-shaped molecule (red line) adsorbed with its symmetry axis tilted compared to the substrate high-symmetry directions. (b) Organizational chirality arises from the molecular arrangement on the surface, illustrated by windmill motifs where the two mirror-image forms have opposite sense of rotation. (c) Prochiral molecules become chiral upon adsorption due to the reduced symmetry following from confinement on the surface. This is illustrated for an L-shaped structure where adsorption leads to two surface enantiomers which can be distinguished by the right/left position of the short leg with respect to the long leg. (d) Conformational chirality may arise for a nonrigid adsorbate. This is illustrated schematically for a hypothetical structure with a “hinge” between its two legs, allowing three different surface conformations to be realized; two chiral enantiomers and one achiral linear form.

plane of the surface (Figure 1b).^{16,17,22} Molecules possessing prochirality become chiral upon adsorption because confinement on the surface reduces their symmetry, leading to the emergence of two mirror image surface enantiomers (Figure 1c).^{7,23–26} In all these cases chiral symmetry is necessarily maintained globally on the surface since mirror image enantiomers/domains are always created in equal proportion. Generally, chiral ordering on surfaces results from molecular diffusion and chiral recognition triggered by intermolecular directional forces and steric constraints. Examples include phase-separation of both intrinsically chiral molecules and molecules possessing prochirality into homochiral^{25,27–29} or enantiomerically enriched²³ domains, chiral amplification by seeding^{21,30} and the formation of homochiral motifs such as molecular wires,^{7,26,31,32} rings,³³ and nanoclusters.³⁴

An additional situation for molecular surface chirality, which we term *conformational chirality*, is illustrated in Figure 1d. Here molecular conformational degrees of freedom enable opposite surface enantiomers to be realized, which is a situation deviating from the typically observed case for prochirality where the surface chirality of rigid, planar compounds is determined simply by which face of the molecule adsorbs toward the surface.^{7,23} Chirality arising solely from the conformation of molecules is not normally considered in organic chemistry since the energy barriers for interconversion between molecular conformers are so low that these are not stable, but conformational chirality has been discussed, for example, for crystal structures and in the context of liquid crystalline assemblies.^{35–37} Molecular conformers may however be stabilized on surfaces due to the molecule–surface interaction, and we tentatively suggest that conformational chirality is quite prone to arise in surface assemblies for appropriate compounds, although this has not to our knowledge been explicitly discussed before.^{5,26,38,39}

We recently synthesized and investigated a molecular model system exhibiting conformational surface

chirality as illustrated in Figure 2a.^{13,40,41} Here, a linear conjugated oligo-(phenylene-ethynylene) (oPE) backbone is equipped with bulky *tert*-butyl groups that are positioned off-axis, leading to two prochiral centers, one at each end of the molecular rod (compare Figure 1c). In the gas phase the shown molecule is achiral since the energy barriers for internal rotations around the ethynylene spokes are low. Once adsorbed on a Au(111) surface, the compound was shown to display conformational chirality in the sense that it can assume two chiral surface enantiomers (marked RR and LL) which are characterized by having their *tert*-butyl groups positioned either to the right (R) or to the left (L), respectively, when looking along the central spoke from the center toward the ends of the molecule. In addition an achiral meso surface form (RL/LR) was realized which has a mirror plane through the center of the molecule, orthogonally to the molecular backbone. Most interestingly, the molecules were shown to undergo thermally induced conformational changes even while adsorbed on the surface, implying that they were able to rotate their end-groups and switch between the displayed chiral and achiral surface forms or between opposite surface enantiomers.⁴⁰ In addition to conformational chirality, the shown compound displayed a highly interesting behavior with respect to organizational chirality by forming two coexisting and distinctly different tiling patterns, one where the molecular backbones assumed a highly symmetric brick-wall stacking as well as a more open grid structure displaying pronounced organizational chirality.

Here we extend this earlier study by synthesizing the entire class of related compounds shown in Figure 2b with systematically varied chemical functionalization of their terminal groups and explore how the associated changes in molecular interactions affect both the organizational and the conformational chirality in molecular self-assembled adsorption structures. Related studies on different geometrical variants of molecules with oPE backbones were recently published

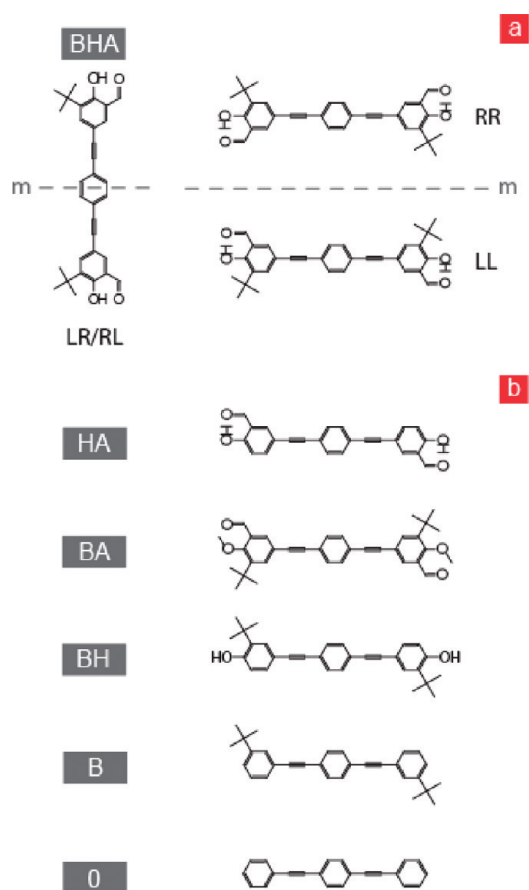


Figure 2. The class of molecules investigated in the present study: (BHA) 1,4-Bis((5-*tert*-butyl-4-hydroxy-3-formylphenyl)ethynyl)benzene. Three different surface conformers LR/RL, RR, and LL can be distinguished by the position left/right (L/R) of the two *tert*-butyl groups when looking from the central benzene ring outward. Note that LR/RL denote the same achiral surface conformer, while RR and LL are enantiomers: (HA) 1,4-bis((3-formyl-4-hydroxyphenyl)ethynyl)benzene; (BA) 1,4-bis((5-*tert*-butyl-3-formyl-4-methoxyphenyl)ethynyl)benzene; (BH) 1,4-bis((2-*tert*-butyl-4-hydroxyphenyl)ethynyl)benzene; (B) 1,4-bis((3-*tert*-butyl-phenyl)ethynyl)benzene; (O) 1,4-bis((phenyl)ethynyl)benzene. The synthesis and characterization of the compounds are described in the Supporting Information.

elsewhere.^{13,41–43} The systematic variations in end-group chemistry aim to (i) modify possible effects of steric hindrance in the molecular tiling by adding/removing the bulky *tert*-butyl group and (ii) modify the ability to form directional intermolecular hydrogen bonds by adding/removing the hydrogen donor (hydroxyl group) and/or the hydrogen acceptor (aldehyde group) of the originally studied compound. By means of high resolution STM we have identified a total of eleven adsorption structures on the Au(111) surface for the six compounds investigated. We analyze these structures with respect to the different levels at which chirality can emerge: point, organizational, and conformational chirality and identify a number of interesting correlations between these. In particular we demonstrate that it is possible through control of the terminal group functionalization to steer the oPE molecular

backbones into surface assemblies that either display pronounced organizational chirality or have mirror symmetric tiling patterns and that it is furthermore possible to control the conformational surface chirality so the compounds preferentially assume either chiral or achiral surface conformers.

RESULTS AND DISCUSSION

In the following we describe the adsorption structures observed for the class of linear oPEs with systematically varied end-group chemistry (Figure 2) upon vacuum sublimation of the molecules onto the noble, inert reconstructed Au(111)-(22 × √3) surface⁴⁴ under clean and well controlled ultrahigh vacuum (UHV) conditions. In the figure panels we display both STM-images and models for the molecular adsorption structures. Ball-models of the underlying Au(111) substrate indicate the molecular dimensions and orientation compared to the substrate, but not registry, which could not be determined, since it was not possible simultaneously to image the adsorption structures and obtain atomic resolution on the Au(111) lattice. Packing densities, unit cell dimensions, and molecular orientations are tabulated.

The chemical names of the investigated molecules are for convenience replaced by systematic abbreviations referring to the functional groups on a given molecule as shown in Figure 2 (B for *tert*-butyl, H for hydroxyl, and A for aldehyde group). The compound without substituents on the backbone is accordingly abbreviated O (zero). Note that in the case of BA the hydroxyl group is not absent but instead it is methylated which will block its ability to act as a hydrogen-bond donor. Synthesis of a compound without the hydroxyl group but with the two other groups retained did not prove feasible.

Scanning tunneling microscopy (STM) images of the adsorption structures were in many instances recorded in two different imaging modes.¹³ In the π -system imaging mode the STM contrast primarily arises from the aromatic molecular backbone leading to three central protrusions (see, e.g., Figure 3a). Hence, the π -system imaging mode enables us to determine the molecular tiling patterns, and thus the organizational chirality of the adsorption structure. In the complementary *tert*-butyl imaging mode (see, e.g., Figure 3b) the topography is dominated by bright protrusions positioned off-axis at the ends of the molecules, which result from the *tert*-butyl functional groups. The *tert*-butyl imaging mode thus enables observation of the molecular conformational chirality and allows assignment of the molecular surface conformations as defined in Figure 2a. The two imaging modes showed no correlation to the tunneling parameters and are ascribed to different STM tip apex terminations which could not be controlled at will.

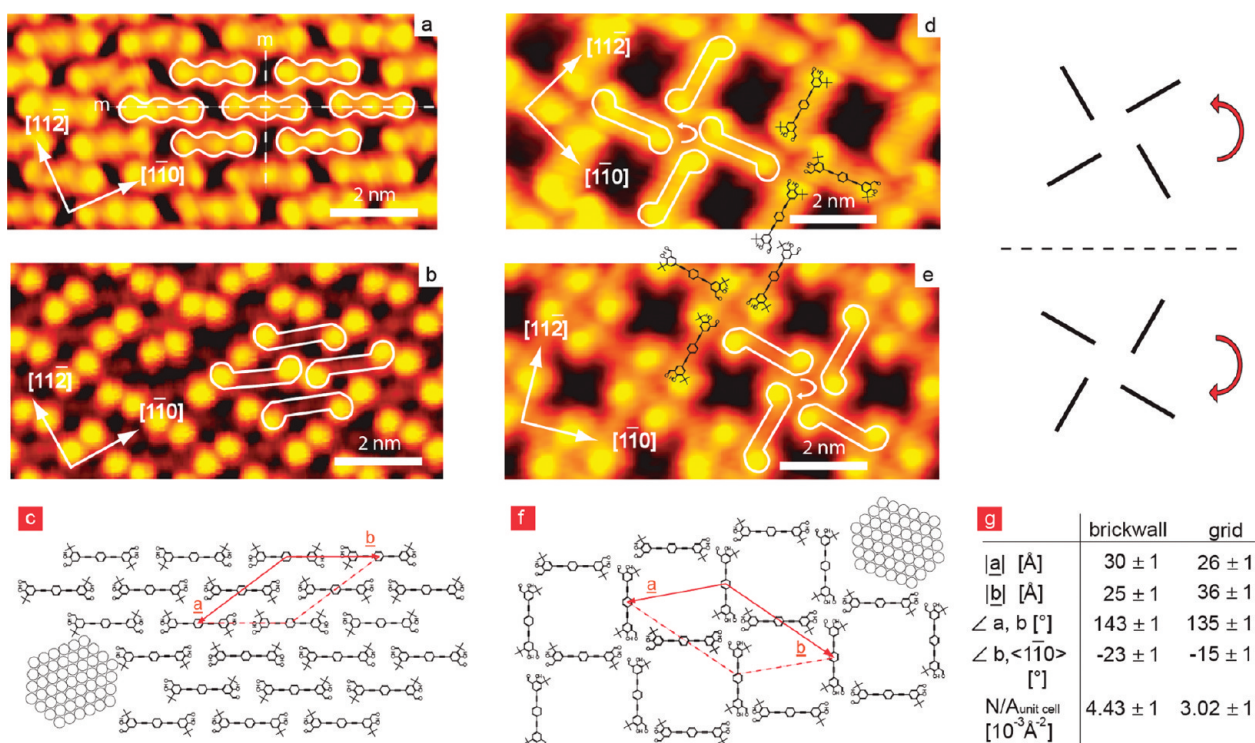


Figure 3. High-resolution STM images and structural models of the brick-wall (a–c) and the grid structure (d–f) formed by **BHA**, obtained in the π -system (a,d) and *tert*-butyl (b,e) imaging modes, respectively. ((a) $I_T = -0.81$ nA; $U_T = -1.25$ V; (b) $I_T = -0.71$ nA; $U_T = -1.25$ V; (c) $I_T = 0.8$ nA; $U_T = 1.25$ V; (d) $I_T = -0.62$ nA; $U_T = -1.05$ V). Molecular models and outlines of the molecular contours in the respective imaging modes are sketched on the STM images to guide the eye. The dashed lines on the brickwall structure in panel a mark mirror planes for the organization of the molecular backbones. Stick models next to the grid structures in panels d and e illustrate that these display organizational chirality and that structures shown in panels d and e are mirror domains. To visualize the orientation of the molecules with respect to the underlying substrate, ball models representing the (111) surface are sketched in the corners of the structural models. Key parameters for the structures are tabulated in panel g.

1,4-Bis(5-*tert*-butyl-4-hydroxy-3-formylphenyl)ethynyl-benzene (BHA). For the originally investigated compound with all three chemical functionalities we observe three distinct adsorption structures, including

the previously described brick-wall and grid structures^{13,40} which are briefly included as follows to facilitate comparison to the other structures observed.

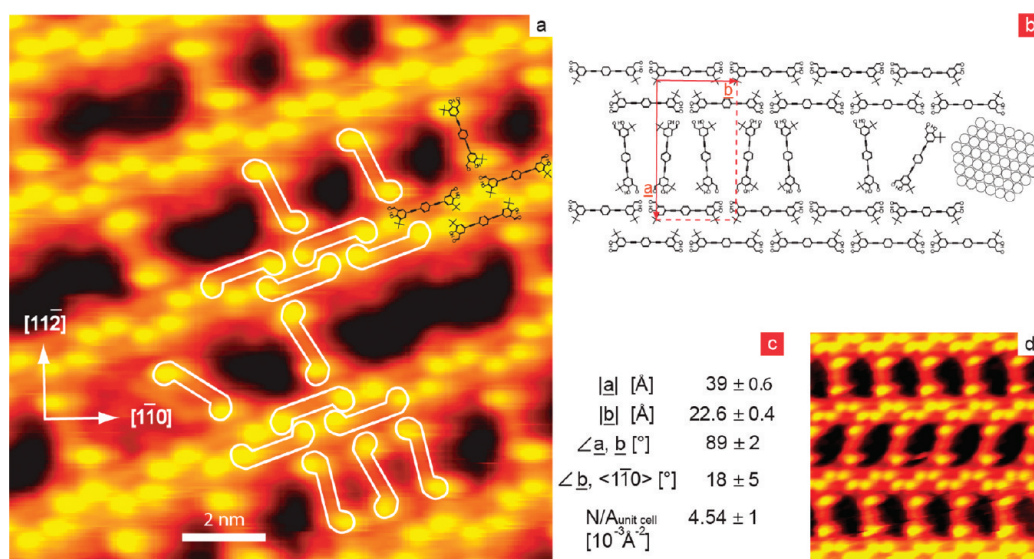
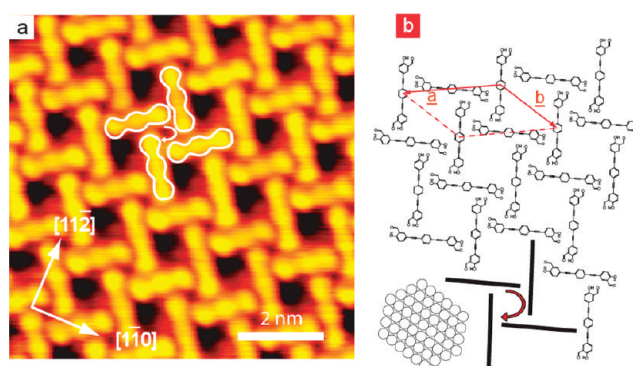


Figure 4. Arcade structure formed by **BHA**. (a) STM image ($I_T = 0.25$ nA; $U_T = 1.4$ V) with overlaid molecular models, and outlines of the molecules as imaged in the *tert*-butyl mode. (b) A model of the adsorption structure with unit cell of the perfect structure. The model also shows molecules in imperfect positions as described in the text. (c) Unit cell dimension, orientation, and packing density of the structure. (d) STM image of an ordered domain in which every second binding position between the rows is occupied.

Brick-Wall Structure. In the brick-wall structure (Figure 3a–c) the molecules close pack efficiently and align head-to-head into parallel rows, as visualized in images obtained in the π -system imaging mode (Figure 3a) showing the benzene rings of the oPE backbone as protrusions. Adjacent rows are shifted relative to each other by half the repeat distance along the rows, analogous to the stacking in a brick wall. The tiling pattern of the molecular backbones is highly symmetric, and the structure therefore does not display organizational chirality. Two mirror planes are sketched in Figure 3a. However, since the molecular backbones are oriented at an angle of $\delta \approx 23^\circ$ with respect to a close packed substrate direction, the molecule–surface system in combination exhibits point chirality. Images of the same structure obtained in the *tert*-butyl imaging mode (Figure 3b) show substantial disorder in the positions of the *tert*-butyl substituents, which appear as bright protrusions. Careful analysis of such images allows the conformation of individual molecules in the structure to be assigned; examples are indicated by outlines in Figure 3b. This reveals that the structure contains both molecules which have assumed the chiral LL or RR conformations as well as molecules in the achiral LR meso form, apparently in a near-random mixture. The structure is thus conformationally disordered.

Grid Structure. Images of the grid structure obtained in the π -system imaging mode (Figure 3d), reveal four molecular backbones meeting in a common node forming a windmill motif. Each molecule connects two such adjacent nodes producing an extended, highly ordered network with nanoscale openings. The grid structure exhibits clear organizational chirality and mirror-image domains with an opposite sense of rotation for the windmill motifs are observed (compare Figure 3 panels d and e). The molecular backbones are oriented at angles of either $\delta \approx 25^\circ$ or $\delta \approx -11^\circ$ to a close packed $\langle 1\bar{1}0 \rangle$ substrate direction and the structure thus also displays point chirality. Images obtained in the *tert*-butyl imaging mode (Figure 3e) show the positions of the *tert*-butyl groups to be completely ordered, in contrast to the situation for the brick-wall structure. The *tert*-butyl groups are always found at the outside of the structural nodes, and domains where molecules order in a clockwise rotating windmill motif are therefore formed exclusively by LL conformers (Figure 3e), and domains with a counter-clockwise rotating windmill motif by RR conformers (Figure 3d). The organizational and conformational chirality is thus perfectly correlated in the grid structure, and the structure consists entirely of the chiral surface conformers which are separated into enantiopure domains.

Arcade Structure. A third adsorption phase combining elements from the predominant *brick-wall* and *grid* structures is occasionally observed (Figure 4). The tiling pattern consists of parallel molecular double rows linked by molecules positioned nearly orthogonal to



$ a $ [Å]	$ b $ [Å]	$\angle a, b$ [°]	$\angle b, \langle 1\bar{1}0 \rangle$ [°]	$N/A_{\text{unit cell}}$ [10^{-3}Å^{-2}]
26.8 ± 0.1	19.4 ± 0.1	136.5 ± 0.9	0 ± 5	5.71 ± 1

Figure 5. Grid structure formed by HA. (a) Highly resolved STM image ($I_T = 0.45$ nA; $U_T = 1.768$ V). Outlines of the molecules are sketched on top of the STM image to guide the eye. A model of the adsorption structure is sketched in panel b. Chiral windmill motifs and the sense of rotation are indicated in panels a and b. To visualize the orientation of the underlying substrate a ball model representing the $\langle 111 \rangle$ surface is sketched in the corner of the structural model. Structural parameters are tabulated in panel c.

these, like the columns of an arcade. In the double rows the molecular tiling is identical to that of the brick-wall structure, that is, two molecular rows are shifted with respect to each other by half the repeat distance along the row. The molecules in the rows are oriented with their backbones at an angle of $\delta \approx 18^\circ$ with respect to a substrate $\langle 1\bar{1}0 \rangle$ direction and all assume a conformation with the *tert*-butyl groups pointing toward the middle of the rows, leading to an optimized packing. As a consequence the double rows are conformationally ordered and consist exclusively of nonchiral LR/RL conformers. The molecules linking the double rows form an angle of $\delta \approx -10^\circ$ with respect to a substrate $\langle 1\bar{1}0 \rangle$ direction and connect to the rows in a motif identical to that assumed in the nodes of the grid structure. The *tert*-butyl groups of the linker molecule thus always point toward the center of the molecule in the double row it connects to, and the linking molecules are exclusively of the chiral RR or LL conformation. At high coverage RR and LL conformers alternate (see unit cell and Figure 4a bottom right) leading to a packing density similar to that found in the brick-wall structure. For a lower coverage only every second binding position between the rows is occupied (Figure 4a top right and Figure 4d) and in this case all the linkers between two rows are of the same chiral conformation. Occasionally we observed achiral LR/RL conformers acting as linkers in which case they were slightly rotated compared to chiral linker molecules indicating that these are stacking faults. The STM image displayed in Figure 4a is chosen to show all possible modifications of this phase. An example of an ordered domain is shown in Figure 4d. In this case the arcade structure is completely con-

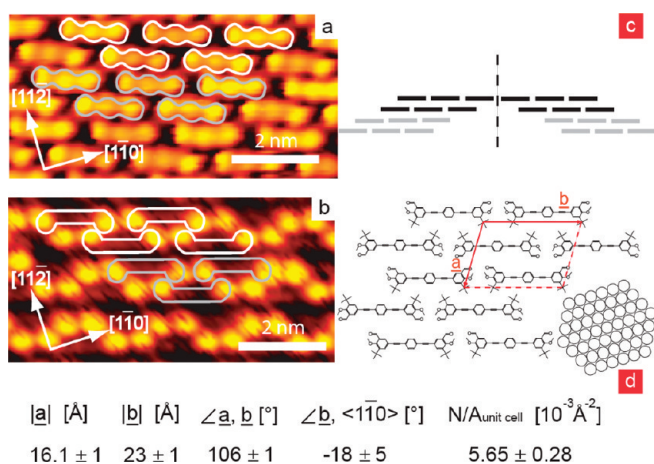


Figure 6. Highly resolved STM images of the brick-wall structure formed by **BA** observed in the π -system (a) and *tert*-butyl (b) imaging modes ((a) $I_T = 1.04$ nA; $U_T = 1.444$ V; (b) $I_T = 0.95$ nA; $U_T = 1.489$ V). Outlines of the molecules are sketched on top of the STM images to guide the eye. The molecular tiling with shifted double rows leads to organizational chirality as indicated in panel c. A model of the adsorption structure as well as a unit cell is sketched in panel d. To visualize the orientation of the underlying substrate a ball model representing the (111) surface is sketched alongside the structural model. Structural parameters are tabulated.

formationally ordered and contains a nonrandom mixture of all three possible molecular conformations—achiral LR/RL in the rows while the gaps between are filled with chiral RR and LL conformers, respectively.

1,4-Bis((3-formyl-4-hydroxyphenyl)ethynyl)benzene—(**HA**).

For the **HA** molecule synthesized without the *tert*-butyl groups, but with the other two types of functional moieties retained, we observed only one adsorption structure.

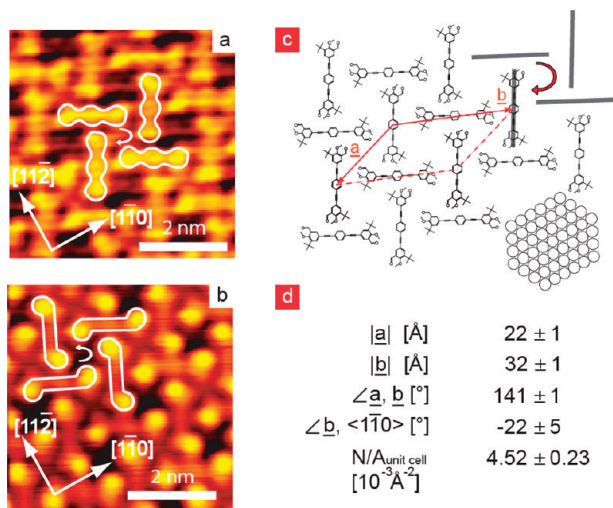


Figure 7. Highly resolved STM images of the gridlike structure formed by **BA** observed in the π -system (a) and *tert*-butyl (b) imaging modes, ((a) $I_T = 1.25$ nA; $U_T = 1.684$ V; (b) $I_T = 1.64$ nA; $U_T = 1.400$ V). Outlines of the molecules are sketched on top of the STM images to guide the eye. A model of the adsorption structure with unit cell is sketched in panel c. To visualize the orientation of the underlying substrate a ball model representing the (111) surface is sketched in the corner of the structural model. Structural parameters are tabulated in panel d.

Grid Structure. As shown in Figure 5a the structure is similar to the grid structure of **BHA** with four molecules meeting in windmill motifs. The orientation of the backbones is similar to the situation for **BHA**, with angles of $\delta \approx 23^\circ$ or $\delta \approx -10^\circ$ to a close packed $\langle 1\bar{1}0 \rangle$ substrate direction. However, in the grid structure for **HA** the molecules are slightly shifted such that their head-groups point more toward the center of neighboring orthogonal backbones, leading to a structure that is closer packed and with smaller pore sizes. The structure is organizationally chiral and mirror-image domains with opposite sense of rotation of the windmill motifs are also observed (not shown). As the **HA** molecules do not contain a *tert*-butyl group they are imaged exclusively in the π -system imaging mode, and it is not possible to determine the conformational chirality of the individual molecules since the aldehyde groups do not provide sufficient contrast to distinguish the two possible rotations of the molecular end-groups. In the model shown in Figure 5b, we assume that the **HA** molecules are in a surface conformation where all the aldehyde groups are oriented toward the central nodes of the structure similar to the case for the **BHA** molecules.

1,4-Bis((5-*tert*-butyl-3-formyl-4-methoxyphenyl)ethynyl)benzene—(BA**).** The **BA** molecule was synthesized with methoxy instead of hydroxyl groups in the para positions of the terminal phenyl rings, and the *tert*-butyl and aldehyde groups were retained. For this compound we observed two adsorption structures, of brick-wall (Figure 6) and grid type (Figure 7), respectively. The two structures were observed to coexist, but the brick-wall structure appeared dominant.

Brick-Wall Structure. In the brick-wall structure the molecules meet head-to-head in parallel rows, and the molecular backbones are oriented at an angle of $\delta \approx 18^\circ$ with respect to a substrate $\langle 1\bar{1}0 \rangle$ direction. In the *tert*-butyl imaging mode (Figure 6b) the rows are observed to pair into double rows in which the *tert*-butyl groups on the participating molecules always point toward the center of the double row, similar to the double rows in the arcade structure for **BHA** (members of two double rows are indicated by white/gray outlines, respectively, in Figures 6a,b). The structure is conformationally ordered, in contrast to the brick-wall structure for **BHA**, and consists exclusively of achiral LR/RL conformers. The two rows of molecules forming a double row are shifted compared to each other by half the repeat distance along the rows similar to the situation for the brick-wall structure formed by **BHA**. However, neighboring double rows are shifted compared to each other by a smaller distance as observed from Figure 6a and the molecular model of Figure 6d. This destroys the mirror symmetry found for the tiling of the molecular backbones in the brickwall structure formed by **BHA** and allows for two mirror-image stacking arrangements as illustrated in Figure 6c, both of which have been ob-

served in STM images. The brick-wall structure for **BA** thus displays organizational chirality and is conformationally ordered involving only the achiral meso RL/LR conformer.

Grid Structure. In the grid structure for **BA** (Figure 7) the molecular backbones form a windmill motif similar to the cases for **BHA** and **HA**. The backbones are nearly orthogonal to each other and oriented at angles of either $\delta \approx -24^\circ$ or $\delta \approx 4^\circ$ with respect to $\langle 1\bar{1}0 \rangle$ substrate directions. Compared to the grid structures of **BHA** and **HA**, the **BA** molecules are shifted such that the end groups point nearly toward the center of a neighboring orthogonal backbone, leading to a higher packing density. As for the other grid structures the tiling pattern of **BA** displays organizational chirality, but it is less pronounced since only a slight further shift of the backbones, causing end groups to point directly toward centers on neighboring molecules, would have rendered the structure mirror symmetric. Similarly to the case for **BHA**, the *tert*-butyl groups of **BA** are always positioned at the outside of the nodes in the grid which renders the structure completely conformationally ordered with enantiopure domains consisting of either RR or LL conformers.

1,4-Bis((2-*tert*-butyl-4-hydroxy)ethynyl)benzene—(BH). The **BH** molecule synthesized without an aldehyde group, but with the *tert*-butyl and hydroxyl groups retained, forms two coexisting structures, one of brick-wall type as well as a new *lamellae* structure with a tiling pattern different from those observed for the previously described compounds.

Brick-Wall Structure. This structure (Figure 8a–c) is very similar to the brickwall structure observed for **BHA**. The backbones of the **BH** molecules form an angle of $\delta \approx 20^\circ$ with a $\langle 1\bar{1}0 \rangle$ substrate direction and the brick-wall tiling pattern of the molecular backbones is achiral. Examples of mirror planes are indicated in Figure 8a. The structure is conformationally disordered and contains both chiral and achiral surface conformers as indicated by outlines in Figure 8a. Accordingly, the structure displays neither conformational ordering nor organizational chirality.

Lamellae Structure. In this structure (Figure 8d–f) the **BH** molecules align side-to-side with parallel backbones forming lamellae running along a substrate $[1\bar{1}0]$ direction. The orientation of the backbones with respect to the substrate alternates between adjacent lamellae with the molecular axis being placed at an angle of $\delta \approx \pm 20^\circ$ with respect to a close packed $\langle 1\bar{1}0 \rangle$ substrate direction. Where the molecular backbones meet head-to-head between lamellae, the *tert*-butyl groups on neighboring molecules are always oriented to the same side. The structure is thus conformationally ordered, and the individual lamellae consist of **BH** molecules entirely in one of the two chiral conformations, RR or LL. The two conformations alternate between adjacent lamellae, creating a racemic mixture of the two

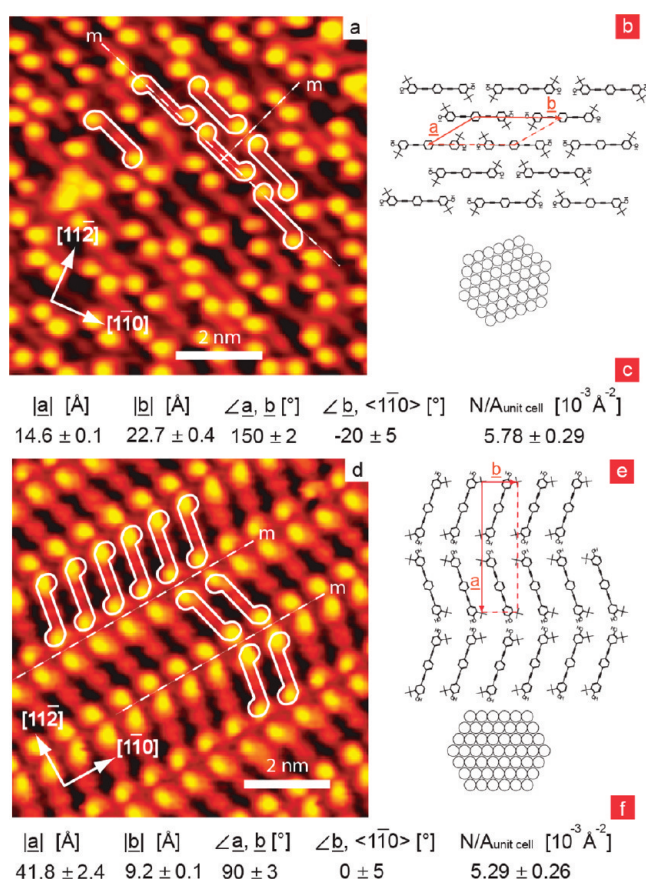


Figure 8. Highly resolved STM images of the brick-wall (a) and lamellae (d) structures formed by **BH** ((a) $I_T = 1.0$ nA; $U_T = 2.102$ V (d) $I_T = -1.34$ nA; $U_T = 2.289$ V). Outlines of the molecules showing the conformational chirality are sketched on top of the STM images to guide the eye. Models of the adsorption structures as well as unit cells are sketched in panels b and e. To visualize the orientation of the underlying substrate ball models representing the (111) surface are sketched at the sides of the structural models. Note that the structural models are rotated compared to the images. Structural parameters are tabulated in panels c and f.

surface enantiomers. The tiling pattern of the molecular backbones contains mirror planes running between the lamellae as indicated in Figure 8d and the structure is thus organizationally achiral. Since the molecular backbones are rotated away from the high symmetry directions of the substrate, the structure locally exhibits point chirality. However, in contrast to all the situations discussed so far, the point chirality does not extend to the entire structure since the indicated mirror plane in this case follows a substrate $[1\bar{1}0]$ direction and the mirror symmetry is thus shared by the molecular tiling pattern and the underlying substrate (strictly this requires an appropriate registry of the molecules with the substrate, but whether this existed could not be ascertained from the STM data). In fact, the mirror symmetry applies even if the molecular conformations are taken into consideration, and very interestingly the lamellae structure therefore appears to be overall achiral when point, organizational, and conformational chirality are considered together.

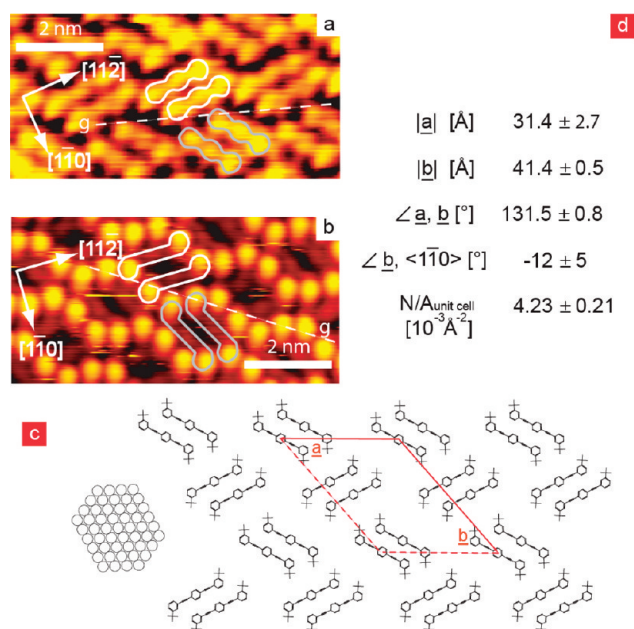


Figure 9. Highly resolved STM images of the pair structure formed by **B** observed in the π -system (a) and *tert*-butyl (b) imaging modes, ((a) $I_T = 0.51$ nA; $U_T = 1.768$ V; (b) $I_T = 0.34$ nA; $U_T = 1.768$ V). Molecular outlines are sketched on top of the STM images to guide the eye. Glideplanes are indicated in panels a and b by white dashed lines. A model of the adsorption structure with unit cell is sketched in panel c. To visualize the orientation of the underlying substrate a ball model representing the (111) surface is sketched at the side of the structural model. Structural parameters are tabulated in panel d.

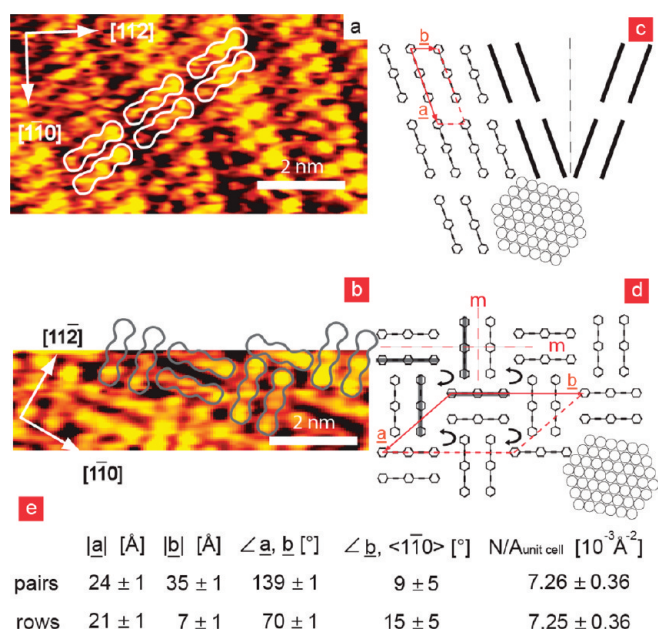


Figure 10. STM images of the row (a) and pair structure (b), formed by the molecular backbone (**O**) alone ((a) $I_T = 0.9$ nA; $U_T = 1.277$ V; (b) $I_T = 0.74$ nA; $U_T = 2.509$ V). Molecular outlines are sketched on top of the STM images to guide the eye. Models of the adsorption structures with unit cells are shown in panels c and d for the row and pair structures, respectively. For the row structure, organizational chirality is indicated by stick models. For the achiral pair structure, different mirror planes and the alternating sense of rotation for neighboring windmill motifs are indicated. Ball models representing the (111) surface are sketched in the corners of the structural model. Structural parameters are tabulated in panel e.

1,4-Bis(3-*tert*-butyl-phenyl)ethynyl)benzene—(B). The compound with only the *tert*-butyl groups connected to the molecular backbone (**B**) is observed to form only one adsorption structure, a *pair* structure (Figure 9), which deviates in its tiling pattern from all the previously described structures.

Pair Structure. STM images obtained in the π -system imaging mode (Figure 9a) reveal that the molecules form molecular pairs in which the backbones are parallel and slightly shifted with respect to each other along the direction of the molecular axis. The **B** pairs adopt two equivalent orientations on the surface with their backbones oriented at angles of $\delta \approx \pm 22^\circ$ with respect to a $\langle 1\bar{1}0 \rangle$ substrate direction. STM images obtained in the *tert*-butyl imaging mode (Figure 9b) show that the **B** pair structure is completely conformationally ordered with a regular arrangement of the protrusions arising from the *tert*-butyl groups. Detailed comparison of STM images obtained in the two imaging modes shows that each pair consists of **B** molecules in the same chiral conformation, either RR or LL. The conformation correlates with the orientation of the pairs such that the rows formed from parallel pairs (running horizontally in Figure 9a) alternate between being formed by molecules in RR and LL conformations, respectively. As a whole the structure is thus conformationally ordered and consists of a racemic mixture of the two chiral surface conformers. The tiling pattern of the molecular backbones is achiral since it contains glideplanes, as illustrated in Figure 9, for which reflection followed by translation along the direction of the plane leads to coincidence. The glide plane is oriented along a substrate $[1\bar{1}0]$ symmetry direction and since mirror image conformational enantiomers are arranged symmetrically on either side of the glide plane, the pair structure as a whole is achiral when all levels of chirality are considered, similar to the situation for the lamellae structure of **BH**.

It may be noticed that the appearance of the pair structure observed in the *tert*-butyl imaging mode (Figure 9b) is superficially very similar to the appearance of the brick-wall structure of **BA** (Figure 6b), but STM images obtained in the π -system imaging mode unambiguously show that the two structures are different which enables a correct assignment of the molecular tiling pattern and conformations.

1,4-Bis(phenyl)ethynyl)benzene—(O). Contrary to the compounds described so far, the molecule without substituents (**O**) is not prochiral. We observed two coexisting adsorption structures, a row structure which has similarities to the lamellae/brickwall structures described above, and a pair structure with resemblance to the pair structure observed for **B**. The data set obtained for **O** is not as detailed as those recorded for the previously described compounds.

Row Structure. In this structure (Figure 10a) the **O** molecules align sideways with parallel backbones into rows. The molecular backbones are tilted by 70° compared

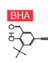
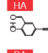
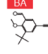
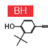
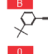
		$\delta_1/^\circ$	$\delta_2/^\circ$	$N/A_{\text{unit cell}} [10^{-3} \text{ \AA}^{-2}]$	conform. chirality	org. chirality
	brickwall	23 ± 5		4.43 ± 0.22	mixed (unordered)	no
	grid	25 ± 5	11 ± 5	3.02 ± 0.15	homochiral (ordered)	yes (windmill)
	arcade	18 ± 5		(4.54 ± 0.23)	mixed (ordered)	no
	grid	23 ± 5	10 ± 5	5.71 ± 0.29	unknown	yes (windmill)
	brickwall	18 ± 5		5.65 ± 0.28	meso (ordered)	yes (shifted brickwall)
	grid	24 ± 5	4 ± 5	4.52 ± 0.23	homochiral (ordered)	yes (windmill)
	lamellae	20 ± 5	20 ± 5	5.29 ± 0.26	racemic (ordered)	no
	brickwall	20 ± 5		5.78 ± 0.29	mixed (unordered)	no
	pair	22 ± 5	22 ± 5	4.23 ± 0.21	racemic (ordered)	no
	pair	18 ± 5	9 ± 5	7.26 ± 0.36	—	no
	row	3 ± 5		7.25 ± 0.36	—	yes (shifted rows)

Figure 11. Overview over observed adsorption structures showing molecular orientations, packing densities as well as the occurrence of conformational and organizational chirality. δ_1 and δ_2 denote the orientation of the molecular backbones with respect to a close packed direction of the Au(111) substrate. Because of the symmetry of the substrate, angles with opposite signs describe the same registry with the substrate. $N/A_{\text{unit cell}}$ denotes the number of molecules in the unit cell divided by the unit cell area and is thus a measure of the packing density.

to the row direction, and form an angle of $\delta \approx -3^\circ$ with respect to a close packed $\langle 1\bar{1}0 \rangle$ direction of the substrate. The molecular orientation does not vary between adjacent rows in contrast to the situation for the **BH** molecule. The structure displays organizational chirality since mirror image domains of the row structure can be formed, as illustrated in Figure 10c.

Pair Structure. In this structure (Figure 10b) the **O** molecules assemble into pairs formed from parallel and aligned backbones. The backbones are rotated by either $\delta \approx 18^\circ$ or $\delta \approx -9^\circ$ with respect to $\langle 1\bar{1}0 \rangle$ substrate directions. Neighboring pairs are oriented orthogonally to each other with the molecular heads of one pair pointing toward the acetylene spokes connecting the center benzene ring with an outer benzene ring of the neighboring molecules. The orthogonal packing of the molecular pairs renders the tiling pattern for the backbones mirror symmetric as indicated in Figure 10d. A windmill motif similar to that formed in the grid phases can be identified for four molecules from adjacent pairs, but in contrast to the grid-structures neighboring windmill nodes have an alternating sense of rotation as indicated in Figure 10d. Hence, the molecular organization does not display organizational chirality.

Overview and Comparison of Adsorption Structures. For the six investigated compounds, a total of 11 adsorption structures are observed on the Au(111) surface. The table in Figure 11 provides an overview over these structures and facilitates comparison of molecular orientations, packing densities and manifestations of conformational and organizational chirality.

Inspection of the packing densities shows that molecules with bulky end groups in general occupy a larger surface area than molecules with less bulky end groups (e.g., **O** compared to **BHA**). However, different molecular structures resulting from the same compound can also vary in packing density, exemplified by the finding that the grid structures formed by the **BHA** and **BA** molecules are less densely packed than the brick-wall structures formed by the same compounds.

The molecular orientations with respect to a close-packed direction on the Au(111) surface fall in two groups with angles between either $\pm 18^\circ$ and $\pm 25^\circ$ or $\pm 3^\circ$ and $\pm 11^\circ$. Within statistical uncertainty this is consistent with two distinct adsorption orientations of $\pm (21 \pm 3)^\circ$ and $\pm (7 \pm 4)^\circ$, respectively. The adsorption orientation of approximately $\pm 21^\circ$ is most abundant since at least one molecule in each unit cell adopts this orientation for all the structures except the row structure formed by **O**. Since these adsorption orientations are adopted irrespectively of the chemical functionalization of the molecules, we conclude that the molecule–substrate orientation is primarily directed by interactions between the substrate lattice and the π -system of the molecular backbone.

In general, the brick-wall and the closely related lamellae structures are formed by molecules containing a *tert*-butyl group and at least one additional group. The packing densities in the brick-wall structures are fairly high compared to the grid structures formed by the same compounds, which suggests that van der Waals interactions contribute significantly to stabilizing the brick-wall structures. Grid structures are formed by three of the compounds, with slight differences in the exact intermolecular arrangement. The packing density for the grid structure formed from **HA** is relatively high compared to the other two grid structures, which is attributed to the absence of the bulky *tert*-butyl group on this compound. For the two grid structures formed by compounds with *tert*-butyl groups, which allow the molecular conformation to be determined, we observe that the participating molecules are completely conformationally ordered. This suggests that relatively strong directional interactions exist between the molecular end-groups. Since the grid structures are formed exclusively by molecules containing an aldehyde group, which is a good hydrogen-bond acceptor, we speculate that all the grid structures are stabilized by directional hydrogen bonds in the nodes of the grid (see Figure 12). The structures formed by the

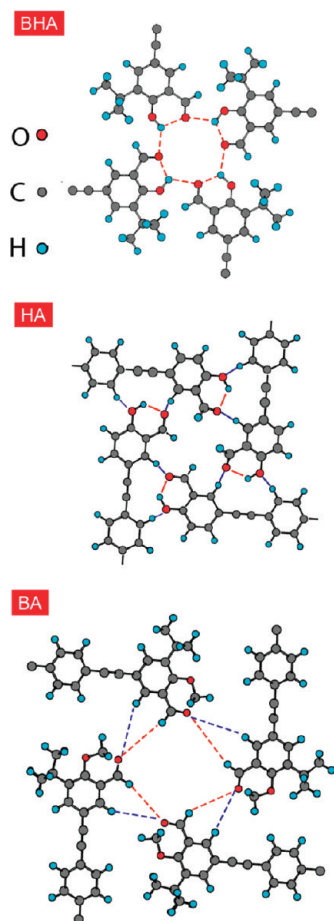


Figure 12. Tentative models showing possible hydrogen-bond configurations in the nodes of the three observed grid structures where the aldehyde groups act as hydrogen acceptors.

pure molecular backbone (**0**) and the *tert*-butyl functionalized backbone (**B**) are characterized by high packing densities with cohesion resulting most likely from van der Waals interactions.

Point and Organizational Chirality. In all the observed structures, the molecular backbones are rotated compared to high symmetry directions of the underlying Au(111) substrate lattice. The molecular adsorption thus breaks the symmetry of the surface, and the single molecules in combination with the surface possess point chirality. In most cases this point chirality extends to entire domains of the molecular adsorption structures, and the molecular tiling pattern within a domain in combination with the atomic lattice displays chirality. This is true, for instance, for all the brick-wall structures. In a few instances, however, the molecular tiling pattern has a mirror or glide plane which falls along a substrate symmetry direction, leading to an overall achiral adsorption structure. This occurs for the lamella structure formed by **BH** and the pair structure formed by **B**.

Organizational chirality, caused by a chiral molecular tiling pattern, is found in several of the structures and is observed to arise in two different ways. Most prominently, the chiral windmill motifs observed in the

grid structures formed for **BHA**, **HA**, and **BA**, can be constructed in two mirror-image forms. Second, in some of the structures dominated by head-to-tail molecular stacking, organizational chirality arises when adjacent rows are neither shifted by a complete nor half a repeat distance along the rows, such that mirror symmetry is avoided. This occurs in the brickwall structure formed by **BA** and the row structure formed by **0**.

Conformational Chirality. Turning to chirality arising from the molecular surface conformations, the variation in terminal group chemistry allows adsorption structures to be formed with a wide range of expressions of conformational chirality. These are summarized in the following in a sequence of increasing conformational and chiral ordering: (i) Conformationally disordered structures which contain a random mixture of the chiral RR, LL, and the achiral RL/LR molecular surface conformations. This situation occurs in the brickwall structures formed by **BHA** and **BH**. (ii) Conformationally ordered structures containing a nonrandom mixture of the chiral, RR, and LL and the achiral RL/LR molecular conformations. This is locally seen in the arcade structure formed by **BHA** where the RL/LR conformers form double rows which are interlinked by RR and LL conformers. (iii) Conformationally ordered structures exclusively built up of the achiral mesocompound, RL/LR, as observed for the brickwall structure formed by **HA**. (iv) Conformationally ordered structures built up of a racemic mixture of the chiral RR and LL surface conformations. This is observed in the lamellae structure formed by **BH** and the pair structure formed by **B**. In these cases each unit cell contains the chiral RR and LL surface conformations in equal proportion. (v) Conformationally ordered structures with separation of the conformational enantiomers into homochiral domains exclusively built up of one of the chiral RR or LL conformers. This is the case for the grid structures formed by **BHA**, **BA**, and potentially also **HA**.

These examples lead to the question how the observed conformational ordering arises dynamically on the surface. Previously, we have shown that the **BHA** compound is able to undergo a thermally activated conformational change in which one of the phenyl end-groups rotates around the axis of the ethynylene spoke, transferring the *tert*-butyl group from one side of the molecular axis to the other, also after adsorption on the Au(111) surface.^{13,40} In Figure 13a, such conformational changes are illustrated by superimposing two time separated STM images colored blue and orange, respectively, such that stationary *tert*-butyl protrusions appear gray, and blue (orange) indicates initial (final) positions of groups that have moved. In addition to **BHA** studied previously, conformational switching is observed in the brick-wall structures formed by **BA** and **BH** as shown in Figure 13a. We therefore assume that all the chemical variants possess the ability to undergo this spontaneous conformational flipping process after

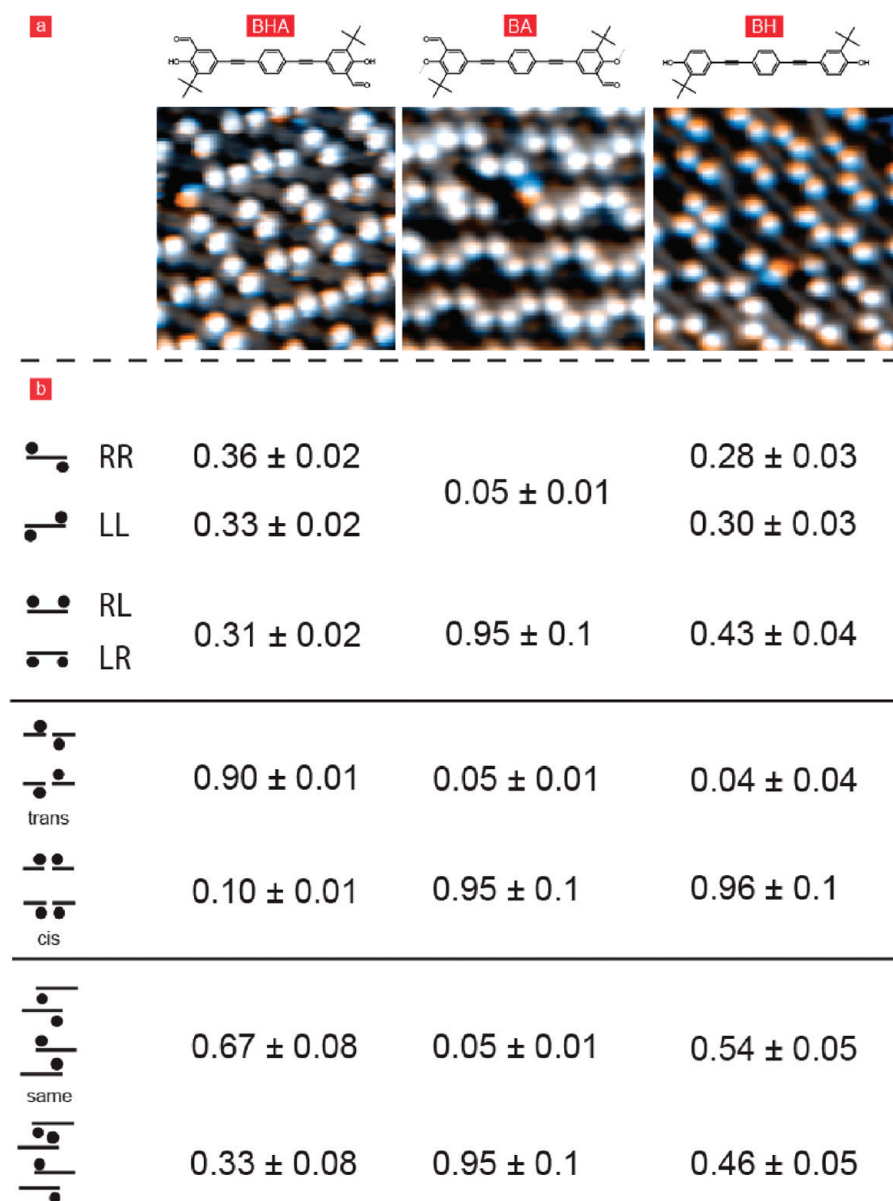


Figure 13. Conformational chirality. (a) STM images revealing conformational changes in the brick-wall structures for the shown compounds. Each panel represents an overlay of two color-coded STM images of the same surface area. Blue (orange) indicates the initial (final) positions of the *tert*-butyl group that change position, whereas stationary groups appear gray. Note that the conformational switch in the highly ordered structure formed by **BA** takes place at the location of a structural defect. (b) Analysis of molecular conformations (chirality) and intermolecular arrangements in the brick-wall structures observed for **BHA**, **BA**, and **BH**. The fractional population of different conformers (top), head-to-head interaction motifs along a row (center), and sideways motifs between rows (bottom) are provided for each of the compounds. The cartoons indicate the position of *tert*-butyl groups with respect to the molecular backbone.

adsorption. This implies that the molecules are not stereochemically fixed on the substrate but can change between the chiral RR and LL conformations and achiral RL/LR surface conformation after adsorption. The molecules can thus dynamically adjust their conformation to the potential-energy landscape experienced during or after condensation into the molecular structures. This opens up a very efficient channel for chiral ordering which we previously termed chiral accommodation. It also implies that the observed structures display a temperature dependent equilibrium (Boltzmann) distribution of surface conformers. The structures with com-

plete conformational/chiral ordering, such as the grid structures and the pair/lamellae structures observed for **B**, thus reflect stronger intermolecular interactions than the structures displaying conformational disorder, and conformational switching is too rare to be observed in these structures. At the boundaries of the molecular islands very high activity is found, but it is difficult to distinguish conformational changes from diffusing molecules.

A particularly interesting case for further analysis occurs for the three brick-wall structures where the molecular tiling patterns are similar, but the degree of confor-

mational ordering is very different. The brick-wall structure formed by **BA** (Figure 6b) has nearly complete conformational order whereas the brick-wall structures formed by **BHA** (Figure 3b) and **BH** (Figure 8d) are more disordered. To understand factors directing the molecular ordering we have quantitatively analyzed the occurrence of different molecular conformations and intermolecular arrangements in these brick-wall structures as summarized in Figure 13b. The first row of the table addresses the statistical occurrence of the different possible surface conformers. Whereas both chiral and achiral surface conformers are present for **BHA** and **BH**, only the achiral RL conformer is realized in the **BA** brick-wall structure. The manifestation of the conformational chirality for the different compounds is thus clearly affected by the functional groups. For the **BHA** and **BH** compounds, respectively, the RR and LL chiral surface conformers occur in equal proportion as expected for reasons of symmetry since the compounds are intrinsically achiral.

The second row of the table addresses interactions between adjacent molecules within a row of the brick-wall structure. Here the *tert*-butyl groups on molecules meeting head to head may be placed either *trans*, at opposite sides of the molecular row, or *cis*, at the same side of the row. All three compounds display an intrarow head-to-head *trans/cis* selectivity of 90% or more at the imaging temperature range of 120–180 K. However, whereas the fully functionalized **BHA** molecules are paired into *trans* head-to-head arrangements, both the **HA** and **BA** molecules favor a *cis* arrangement. This is also observed in the lamellae structure formed by **BA** where the relative tilt between neighboring molecules within a row potentially leads to an even stronger interaction. Furthermore, the regularity of the inter-row molecular arrangements depends on the compounds (second row in Figure 13b), with a partial preference for ordering toward a *same* side arrangement observed for **BHA**, no selectivity observed for **HA** and a complete ordering toward an *opposite* side arrangement found for **BA**. The compound **BA**, which is conformationally ordered, is thus the only compound of the three displaying nearly complete regularity in both intrarow and inter-row arrangements with respect to neighboring molecules. We thus conclude that the interplay between the intra-row and inter-row interactions in the specific adsorption structure is responsible for steering of the **BA** compound to assume fully achiral surface conformers. We speculate that the intra-row ordering is controlled by directional interactions between the functional end-groups, whereas the inter-row ordering is controlled by weaker interactions (potentially weak hydrogen bonds) between hydrogen atoms on the aromatic backbones and the aldehyde groups.

Correlation between the Levels of Chirality. From the analysis presented here, many examples are found of corre-

lation between the different levels at which chirality can arise in the molecular surface assemblies; point chirality as extended to the entire structures, organizational chirality, and conformational chirality. These fall in three main classes. (i) Highly ordered structures which are built up of only a single surface conformer (i.e., homochiral structures and pure meso structures) possess both organizational chirality and extended point chirality. This category includes the homochiral grid structures formed by **BHA**, **HA**, and **BA** and the brickwall structure formed by the meso conformation of **BA**. In particular, we see that the perfect grid structures express chirality at all levels and the conformational and organizational chirality is directly correlated by the requirement that the *tert*-butyl substituents are always placed at the outside of the nodes in the windmill motifs. (ii) In contrast, purely racemic structures built up of the RR and LL conformation in an equal proportion are completely achiral in that they neither possess organizational chirality nor extended point chirality. This occurs for the lamellae structure formed by **BH** and the pair structure formed by **B**. (iii) Finally, conformationally disordered structures built up of a random mixture of the three surface conformations do possess extended point chirality but not organizational chirality. This situation occurs for the brick-wall structures formed by **BHA** and **BH**.

CONCLUSIONS

We have synthesized a class of linear oligophenylene-ethynylenes with systematic variations in the chemical functionality of their terminal groups and characterized the adsorption structures formed by these compounds on the Au(111) surface using high-resolution STM under UHV conditions. Two main types of adsorption structures are observed recurrently, either close-packed brick-wall/lamellae/row structures or grid structures with molecules arranged in a characteristic windmill motif. A number of trends for how the chemical functionalization directs formation of these different structures have been identified; in particular are grid structures observed when the molecular functionalization allows for directional hydrogen bonding.

All of the investigated compounds are intrinsically achiral, but most are prochiral, and chirality is manifested repeatedly in the observed supramolecular structures. This occurs as point chirality, as organizational chirality expressed in the tiling of the molecular backbones, and as conformational chirality expressed in the molecular adsorption conformation where the terminal groups can be rotated to realize either an achiral meso form or one of two opposite chiral surface enantiomers. Different STM imaging modes highlighting the molecular backbones or the bulky *tert*-butyl substituents, respectively, allow the organizational and conformational chirality to be directly identified. A range of different situations are found with respect to conforma-

tional chirality in the observed structures, spanning from conformationally disordered structures, over conformationally ordered structures involving either the achiral meso compound or both chiral enantiomers, to structures with homochiral domains involving only one of the conformational enantiomers. The different levels of chirality expressed in the structures are found to be strongly correlated: Structures with domains that are conformationally homochiral display both organizational and point chirality as exemplified, for example, by the grid structures observed for **BHA** and **BA**. In contrast, structures with domains that are conformationally racemic do not display organizational chirality and the point chirality is canceled by symmetry elements shared by the molecular tiling pattern and the substrate, as observed for the pair and lamellae structures formed by **B** and **BH**, respectively. Most importantly we find that the molecular design offers control over the

different expressions of chirality, which can be steered by tuning the chemical functionality of the terminal groups without explicitly introducing chiral substituents. The organizational chirality can thus be steered by choosing the end group functionalization such that either chiral windmill or achiral brick-wall/lamellae tiling motifs are formed as shown by comparison of the results for **HA** and **BH**. The preferential formation of chiral or achiral surface conformers can furthermore be controlled as shown by comparison of the brick-wall structures for **BHA**, **BH**, and **BA**. In all the investigated situations chiral symmetry is necessarily maintained globally on the surface since all the compounds are intrinsically achiral. Further studies are presently being undertaken to explore if and how this symmetry can be broken by augmenting the investigated class of compounds by members functionalized by appropriate chiral substituents.

EXPERIMENTAL METHODS

The experiments were performed in two UHV-chambers with base pressures in the low 10^{-10} mbar region, both equipped with standard facilities for sample preparation and characterization as well as the home-built, variable temperature Aarhus Scanning Tunneling Microscope (STM).⁴⁵ Cleaning of the Au(111) single crystal surfaces was performed by repeated cycles of sputtering with Ar⁺ ions at 1.5 keV for 20 min and an ion current density of approximately $1 \mu\text{A}/\text{cm}^2$ followed by annealing to 850 K for 10 min while limiting the temperature ramps to ± 100 K/min.

The molecules are synthesized in our organic chemistry laboratory, except for 1,4-bis((phenyl)ethynyl)benzene which was purchased from Sigma Aldrich. The general synthetic approach to **BHA**, **HA**, **BA**, **BH**, and **B** has been to prepare or purchase the terminal aromatic groups containing a iodo- or bromosubstituent in the required position. The terminal groups were coupled to the central 1,4-diethynylbenzene in a Sonogashira cross coupling reaction. Protection of the aldehyde and the phenol during the synthesis of compound **HA** was required to increase the solubility of the intermediates. A detailed description of the organic synthesis and characterization is given in the Supporting Information. All the resulting products **BHA**, **HA**, **BA**, **BH**, **B**, and **O** are solids at room temperature.

Prior to evaporation of the molecules onto the Au(111) surface in the UHV chamber, the compounds were ground into a powder and loaded in a glass crucible wound with a thin metal wire for resistive heating. The crucible temperature was monitored with a NiCr/Ni thermocouple pair melted into the glass. The six compounds were sublimated in submonolayer quantities at a compound specific temperature in the range of 80–140 °C. Prior to evaporation the powder was thoroughly outgassed. The molecules were deposited onto a clean Au(111) sample held at room temperature (~ 300 K). To stabilize the adsorption structures the sample was subsequently cooled to lower temperatures (120–180 K) prior to imaging with the STM. For some of the compounds the influence of the cooling rate on the resulting molecular structures was tested by performing both a rapid quenching (inserting the room temperature sample directly into the precooled STM) and a slow cool down over a period of more than 30 min from room temperature to the imaging temperature. No significant differences were found between the two methods, showing that the observed structures are not kinetically trapped.

The lateral calibration of the STM images was performed from atomic resolution STM images of the Au(111) surface. In some cases the known length of a molecular feature, determined from independently calibrated images, was used to obtain an even better precision in calibration of specific STM images. For

a few cases it was necessary to correct recorded STM images for thermal drift within the x – y -plane when determining unit cell vectors. For this purpose a drift vector was determined from two consecutive high resolution STM images of the adsorption structure containing an appropriate marker. The errors specified for lengths and angles of unit cell vectors are statistical in cases where several STM images were available for analysis. In the case of a more limited data set, an uncertainty of $\pm 5\%$ was assumed. Possible systematic errors in the calibration process were not taken into account, but we estimate the total precision in the quoted dimensions to be better than 10% in all cases.

To compare the different adsorption structures, a molecular packing density was determined by dividing the number N of molecules per unit cell by the area A_{unitcell} of the unit cell. The orientation of molecules and unit cell vectors with respect to close packed $\langle 1\bar{1}0 \rangle$ directions of the Au(111) substrate was determined to a precision of $\pm 5^\circ$ by comparison to atomic resolution images of the substrate. Angles between the vectors **a** and **b** ($= \angle \mathbf{a}, \mathbf{b}$) are counted positive if a clockwise rotation of vector **a** decreases this angle. However, due to the symmetry of substrate and molecules the distribution of specific adsorption places is independent of the sign of this angle.

ACKNOWLEDGMENT Eva Rauls and Bjørk Hammer are acknowledged for helpful discussions. We also acknowledge the financial support from the EU programs PICO-INSIDE, FUN-SMARTS, and MONET as well as from the Danish Natural Science Research Council, the Danish Ministry for Science and Innovation for support to iNANO, and the Carlsberg Foundation and the Danish National Research Foundation for support to CDNA.

Supporting Information Available: Details of the organic synthesis. This material is available free of charge via the Internet at <http://pubs.acs.org>.

REFERENCES AND NOTES

- Barth, J. V. Molecular Architectonic on Metal Surfaces. *Annu. Rev. Phys. Chem.* **2007**, *58*, 375–407.
- Ernst, K. H. In Supramolecular Surface Chirality. *Top. Curr. Chem.* **2006**, *265*, 209–252.
- Barlow, S. M.; Raval, R. Complex Organic Molecules at Metal Surfaces: Bonding, Organisation, and Chirality. *Surf. Sci. Rep.* **2003**, *50*, 201–341.
- Yokoyama, T.; Yokoyama, S.; Kamikado, T.; Okuno, Y.; Mashiko, S. Selective Assembly on a Surface of Supramolecular Aggregates with Controlled Size and Shape. *Nature* **2001**, *413*, 619–621.

- Llanes-Pallas, A.; Matena, M.; Jung, T.; Prato, M.; Stöhr, M.; Bonifazi, D. Trimodular Engineering of Linear Supramolecular Miniatures on Ag(111) Surfaces Controlled by Complementary Triple Hydrogen Bonds. *Angew. Chem., Int. Ed.* **2008**, *47*, 7726–7730.
- Barth, J. V.; Weckesser, J.; Cai, C. Z.; Günter, P.; Bürgi, L.; Jeandupeux, O.; Kern, K. Building Supramolecular Nanostructures at Surfaces by Hydrogen Bonding. *Angew. Chem., Int. Ed.* **2000**, *39*, 1230–1234.
- Chen, Q.; Richardson, N. V. Enantiomeric Interactions between Nucleic Acid Bases and Amino Acids on Solid Surfaces. *Nat. Mater.* **2003**, *2*, 324–328.
- Dmitriev, A.; Lin, N.; Weckesser, J.; Barth, J. V.; Kern, K. Supramolecular Assemblies of Trimesic Acid on a Cu(100) Surface. *J. Phys. Chem. B* **2002**, *106*, 6907–6912.
- Stöhr, M.; Wahl, M.; Galka, C. H.; Riehm, T.; Jung, T. A.; Gade, L. H. Controlling Molecular Assembly in Two Dimensions: The Concentration Dependence of Thermally Induced 2D Aggregation of Molecules on a Metal Surface. *Angew. Chem., Int. Ed.* **2005**, *44*, 7394–7398.
- Pawin, G.; Wong, K. L.; Kwon, K. Y.; Bartels, L. A. Homomolecular Porous Network at a Cu(111) Surface. *Science* **2006**, *313*, 961–962.
- Otero, R.; Schöck, M.; Molina, L. M.; Lægsgaard, E.; Stensgaard, I.; Hammer, B.; Besenbacher, F. Guanine Quartet Networks Stabilized by Cooperative Hydrogen Bonds. *Angew. Chem., Int. Ed.* **2005**, *44*, 2270–2275.
- Ma, J.; Rogers, B. L.; Humphry, M. J.; Ring, D. J.; Goretzki, G.; Champness, N. R.; Beton, P. H. Dianhydride–Amine Hydrogen Bonded Perylene Tetracarboxylic Dianhydride and Tetraaminobenzene Rows. *J. Phys. Chem. B* **2006**, *110*, 12207–12210.
- Busse, C.; Weigelt, S.; Petersen, L.; Lægsgaard, E.; Besenbacher, F.; Linderoth, T. R.; Thomsen, A. H.; Nielsen, M.; Gothelf, K. V. Chiral Ordering and Conformational Dynamics for a Class of Oligo-phenylene-ethynylenes on Au(111). *J. Phys. Chem. B* **2007**, *111*, 5850–5860.
- Gross, L.; Moresco, F.; Ruffieux, P.; Gourdon, A.; Joachim, C.; Rieder, K. H. Tailoring Molecular Self-Organization by Chemical Synthesis: Hexaphenylbenzene, Hexa-peri-hexabenzocoronene, and Derivatives on Cu(111). *Phys. Rev. B* **2005**, *71*, 165428.
- Swarbrick, J. C.; Ma, J.; Theobald, J. A.; Oxtoby, N. S.; O'Shea, J. N.; Champness, N. R.; Beton, P. H. Square, Hexagonal, and Row Phases of PTCDA and PTCDI on Ag-Si(111) $\sqrt{3} \times \sqrt{3} R30^\circ$. *J. Phys. Chem. B* **2005**, *109*, 12167–12174.
- Schöck, M.; Otero, R.; Stojkovic, S.; Hümmelink, F.; Gourdon, A.; Lægsgaard, E.; Stensgaard, I.; Joachim, C.; Besenbacher, F. Chiral Close-Packing of Achiral Star-Shaped Molecules on Solid Surfaces. *J. Phys. Chem. B* **2006**, *110*, 12835–12838.
- de Wild, M.; Berner, S.; Suzuki, H.; Yanagi, H.; Schlettwein, D.; Ivan, S.; Baratoff, A.; Güntherodt, H. J.; Jung, T. A. A Novel Route to Molecular Self-Assembly: Self-Intermixed Monolayer Phases. *Chemphyschem* **2002**, *3*, 881–885.
- Lopinski, G.; Moffatt, D.; Wayner, D.; Wolkow, R. Determination of the Absolute Chirality of Individual Adsorbed Molecules Using the Scanning Tunneling Microscope. *Nature* **1998**, *392*, 909–911.
- Lorenzo, M. O.; Baddeley, C. J.; Muryrn, C.; Raval, R. Extended Surface Chirality from Supramolecular Assemblies of Adsorbed Chiral Molecules. *Nature* **2000**, *404*, 376–379.
- Kühnle, A.; Linderoth, T. R.; Hammer, B.; Besenbacher, F. Chiral Recognition in Dimerization of Adsorbed Cysteine Observed by Scanning Tunneling Microscopy. *Nature* **2002**, *415*, 891–893.
- Parschau, M.; Romer, S.; Ernst, K. H. Induction of Homochirality in Achiral Enantiomorphous Monolayers. *J. Am. Chem. Soc.* **2004**, *126*, 15398–15399.
- Qiu, X. H.; Wang, C.; Zeng, Q. D.; Xu, B.; Yin, S. X.; Wang, H. N.; Xu, S. D.; Bai, C. L. Alkane-Assisted Adsorption and Assembly of Phthalocyanines and Porphyrins. *J. Am. Chem. Soc.* **2000**, *122*, 5550–5556.
- Böhringer, M.; Morgenstern, K.; Schneider, W. D.; Berndt, R. Separation of a Racemic Mixture of Two-Dimensional Molecular Clusters by Scanning Tunneling Microscopy. *Angew. Chem., Int. Ed.* **1999**, *38*, 821–823.
- Bonello, J. M.; Williams, F. J.; Santra, A. K.; Lambert, R. M. Fundamental Aspects of Enantioselective Heterogeneous Catalysis: The Surface Chemistry of Methyl Pyruvate on Pt{111}. *J. Phys. Chem. B* **2000**, *104*, 9696–9703.
- France, C. B.; Parkinson, B. A. Naphtho[2,3-a]pyrene Forms Chiral Domains on Au(111). *J. Am. Chem. Soc.* **2003**, *125*, 12712–12713.
- Weckesser, J.; Vita, A. D.; Barth, J. V.; Cai, C.; Kern, K. Mesoscopic Correlation of Supramolecular Chirality in One-Dimensional Hydrogen-Bonded Assemblies. *Phys. Rev. Lett.* **2001**, *87*, 096101.
- Fasel, R.; Parschau, M.; Ernst, K.-H. Chirality Transfer from Single Molecules into Self-Assembled Monolayers. *Angew. Chem., Int. Ed.* **2003**, *42*, 5177–5181.
- Vidal, F.; Delvigne, E.; Stepanow, S.; Lin, N.; Barth, J. V.; Kern, K. Chiral Phase Transition in Two-Dimensional Supramolecular Assemblies of Prochiral Molecules. *J. Am. Chem. Soc.* **2005**, *127*, 10101–10106.
- Stepanow, S.; Lin, N.; Vidal, F.; Landa, A.; Ruben, M.; Barth, J. V.; Kern, K. Programming Supramolecular Assembly and Chirality in Two-Dimensional Dicarboxylate Networks on a Cu(100) Surface. *Nano Lett.* **2005**, *5*, 901–904.
- Fasel, R.; Parschau, M.; Ernst, K. H. Amplification of Chirality in Two-Dimensional Enantiomorphous Lattices. *Nature* **2006**, *439*, 449–452.
- Schiffirin, A.; Riemann, A.; Auwärter, W.; Pennec, Y.; Weber-Bargioni, A.; Cvetko, D.; Cossaro, A.; Morgante, A.; Barth, J. V. Zwitterionic Self-Assembly of L-Methionine Nanogratings on the Ag(111) surface. *Proc. Natl. Acad. Sci. U.S.A.* **2007**, *104*, 5279–5284.
- Böhringer, M.; Morgenstern, K.; Schneider, W. D.; Berndt, R.; Mauri, F.; De Vita, A.; Car, R. Two-Dimensional Self-Assembly of Supramolecular Clusters and Chains. *Phys. Rev. Lett.* **1999**, *83*, 324–327.
- Blüm, M. C.; Cavar, E.; Pivetta, M.; Patthey, F.; Schneider, W. D. Conservation of Chirality in a Hierarchical Supramolecular Self-Assembled Structure with Pentagonal Symmetry. *Angew. Chem., Int. Ed.* **2005**, *44*, 5334–5337.
- Kühnle, A.; Linderoth, T. R.; Besenbacher, F. Self-Assembly of Monodispersed, Chiral Nanoclusters of Cysteine on the Au(110)-(1 × 2) Surface. *J. Am. Chem. Soc.* **2003**, *125*, 14680–14681.
- Dodziuk, H. Chirality and Stereogenicity—The Importance of Conformational Chirality in the Classification of Stereoisomers. *Tetrahedron Asymmetry* **1992**, *3*, 43–50.
- Walba, D. M.; Korblova, E.; Huang, C. C.; Shao, R. F.; Nakata, M.; Clark, N. A. Reflection Symmetry Breaking in Achiral Rod-Shaped Smectic Liquid Crystals? *J. Am. Chem. Soc.* **2006**, *128*, 5318–5319.
- Sekine, T.; Niori, T.; Sone, M.; Watanabe, J.; Choi, S. W.; Takanishi, Y.; Takezoe, H. Origin of Helix in Achiral Banana-Shaped Molecular Systems. *Jpn. J. Appl. Phys.* **1997**, *36*, 6455–6463.
- Henzl, J.; Mehlhorn, M.; Gawronski, H.; Rieder, K. H.; Morgenstern, K. Reversible Cis–Trans Isomerization of a Single Azobenzene Molecule. *Angew. Chem., Int. Ed.* **2006**, *45*, 603–606.
- Miwa, J. A.; Weigelt, S.; Gersen, H.; Besenbacher, F.; Rosei, F.; Linderoth, T. R. Azobenzene on Cu(110): Adsorption Site-Dependent Diffusion. *J. Am. Chem. Soc.* **2006**, *128*, 3164–3165.
- Weigelt, S.; Busse, C.; Petersen, L.; Rauls, E.; Hammer, B.; Gothelf, K. V.; Besenbacher, F.; Linderoth, T. R. Chiral Switching by Spontaneous Conformational Change in Adsorbed Organic Molecules. *Nat. Mater.* **2006**, *5*, 112–117.
- Weigelt, S.; Busse, C.; Bombis, C.; Knudsen, M.; Martin, M.; Gothelf, K. V.; Strunskus, T.; Wöll, C.; Dahlbom, M.; Hammer, B.; Lægsgaard, E.; Besenbacher, F.; Linderoth,

- T. R. Covalent Interlinking of an Aldehyde and an Amine on a Au(111) Surface in Ultrahigh Vacuum. *Angew. Chem., Int. Ed.* **2007**, *46*, 9227–9230.
42. Weigelt, S.; Busse, C.; Nielsen, M.; Gothelf, K. V.; Lægsgaard, E.; Besenbacher, F.; Linderoth, T. R. Influence of Molecular Geometry on the Adsorption Orientation for Oligophenylene–Ethylenes on Au(111). *J. Phys. Chem. B* **2007**, *111*, 11342–11345.
43. Weigelt, S.; Bombis, C.; Busse, C.; Knudsen, M. M.; Gothelf, K. V.; Lægsgaard, E.; Besenbacher, F.; Linderoth, T. R. Molecular Self-Assembly from Building Blocks Synthesized on a Surface in Ultrahigh Vacuum: Kinetic Control and Topo-Chemical Reactions. *ACS Nano* **2008**, *2*, 651–660.
44. Barth, J. V.; Brune, H.; Ertl, G.; Behm, R. J. Scanning Tunneling Microscopy Observations on the Reconstructed Au(111) Surface: Atomic Structure, Long-Range Superstructure, Rotational Domains, and Surface Defects. *Phys. Rev. B* **1990**, *42*, 9307–9318.
45. Lægsgaard, E.; Besenbacher, F.; Mortensen, K.; Stensgaard, I. A Fully Automated, Thimble-Size Scanning Tunneling Microscope. *J. Microsc.* **1988**, *152*, 663–669.